Finite Difference Solution for a Transient Temperature Distribution in an Advanced Polymer Fiber

Parham Sadooghi, Cyrus Aghanajafi

K.N.T University of Technology, Tehran, Iran

Received 24 November 2004; accepted 25 June 2005
DOI 10.1002/app.23575
Published online in Wiley InterScience (www.interscience.wiley.com).

ABSTRACT: A model is presented for the calculation of transient combined radiative and conductive heat transfer in a semitransparent layer of advanced fiber polymer. This model is based on optical material properties. Different boundary conditions were examined. Each side of the layer was exposed to hot or cold radiative surroundings, whereas each boundary was heated or cooled by convection. Emission within the layer and internal reflections depended on the layer refractive index. The reflected energy and heat conduction distributed energy across the layer and partially equalized the transient temperature distributions. The numerical method is an implicit finite difference procedure with nonuniform space and time increments that has been expanded to include external convection and incident radiation. © 2006 Wiley Periodicals, Inc. J Appl Polym Sci 100: 4181–4189, 2006

Key words: transient temperature; fibers

INTRODUCTION

Interest in advanced fibers derived from synthetic organic polymers has grown substantially over the past 20 years. Underlying this growth is the remarkable range of mechanical and thermal properties exhibited by advanced fibers; this range permits their use for a variety of purposes. These properties may include having high-temperature strength, high stiffness, low moisture, absorption, no creep, and being light in weight. Because of the widespread use of advanced fibers, there has been considerable interest in the problem of heat transfer through synthetic organic polymers. They can be subjected to transient heating or cooling by a variety of external radiation and convection conditions, some of which are partially transparent to radiative energy. Within the material, radiative transport acts in combination with heat conduction. Because the materials operate at high temperatures, there is a considerable amount of internal emissions, which is proportional to the layer refractive index squared. Polymer refractive indices range from approximately 1 to 3, so internal radiation fluxes can be large. Because these fluxes depend strongly on temperature, accurate instantaneous temperature distributions must be calculated during a transient numerical solution, or the heat flows and hence the solution becomes inaccurate over time.

Correspondence to: P. Sadooghi (parhampari2002@yahoo.com).

Journal of Applied Polymer Science, Vol. 100, 4181–4189 (2006)

Within a polymer fiber, energy can be transferred internally by radiation in addition to by heat conduction. Because radiant propagation is very rapid, it can provide energy in the material more quickly than can diffusion by heat conduction.[1] The behavior of these kinds of polymers is influenced by their surroundings, in which they can be heated internally by incident radiation or they can lose energy internally by radiation to a cooler environment, and the radiative surroundings can provide a positive or negative internal heat source.[2] Convective heating or cooling can also be applied at the boundaries, and radiant effects are accentuated as there is a rise in temperature, which can be the temperature of the material, the temperature of the surroundings, or both. An example is heating a plastic with infrared lamps to soften it for a manufacturing process.[3] If the material is hot, there are also significant internal emissions. Each part of the volume emits radiation, which is transmitted to the other locations within the material, where it is partially absorbed.[4] The ability to transfer to other locations depends on the transparency of the material. If the material is not very transparent, radiation will pass only to nearby locations before being absorbed. It can then continue along its journey by being emitted again.

Fiber polymers are widely used in various high-temperature applications including thermal insulation of furnaces and heat exchangers.[5–7] Their application in the electrical and electronic industries is especially important because this has enabled a real increase in the reliability of electrical machines and the development of materials for ICs and microelectronics. They also are used in thermal protection systems[4] and other

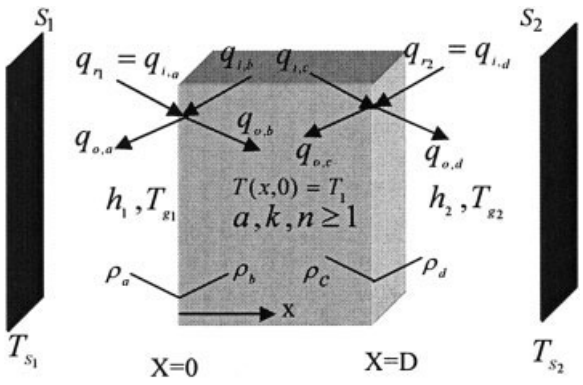

Figure 1 Geometry, boundary conditions, and nomenclature for plane layer with externally incident radiation and surface convection.

industrial equipment, and in aircraft, automotive engines, and even sporting goods. Because temperature responses including radiation can be significantly different from those by conduction alone, detailed transient solutions are necessary to examine heat transfer for insulation systems and ignition and flame spread for different kinds of plastics.

Lists of previous works on combined radiation and conduction heat transfer can be found in a review article[8] and a textbook.[9] Although there have been far fewer studies of transient behavior, existing works have analyzed a variety of situations for single and multiple layers.[10–18] Several excellent reviews on radiation and combined radiation and conduction energy transfer in dispersed media are available.[19–22] Many previous studies considered the problems of heat transfer in glass-fiber insulation.[23]

This article presents an investigation of the transient behavior of a nongray layer, particularly, advanced polymers, held at high temperature and subjected to various radiative (opaque or transparent, specular or diffuse) and thermal boundary (first, third, and mixed) conditions. The numerical method is an implicit finite difference procedure with nonuniform space and time increments. The basic method, developed in a previous work,[3] has been expanded to include external convection and incident radiation.

EXPERIMENTAL

Energy equation

A flat-layered homogeneous, isotropical, gray-emitting material that was absorbent and nonscattering with D thickness was considered (Fig. 1). The layer was heat conducting and had a refractive index of $n \geq 1$. Initially, the layer was at a uniform temperature, T_i, so $t(X,0) = 1$. It was then placed in surroundings where it could receive radiant energy, q_{r1} and q_{r2}, on each side. The layer also could be cooled or heated on each side by the surrounding gas at temperatures T_{s1} and T_{s2} with heat transfer coefficients h_1 and h_2.

The general energy equation for transiently coupled heat transfer in dimensionless form is[24]:

$$\frac{\partial t}{\partial \tau} = N\frac{\partial^2 t}{\partial X^2} - R(t) \tag{1}$$

where $R(t)$ is the gradient of the radiative flux and a function of X and τ,

$$R(t) \equiv n^2\kappa_D T^a(X,\tau) - \frac{\kappa_D}{2}\{\tilde{q}_{0,b}(\tau)E_2(\kappa_D X) + \tilde{q}_{0,c}(\tau)E_2[\kappa_D(1-X) + n^2\kappa_D\int_0^4 t^4(X^+,\tau)E_1\kappa_D|X^+ - X|dX^+\} \tag{2}$$

where $\tilde{q}_{0,b}$ and $\tilde{q}_{0,c}$ are dimensionless diffuse fluxes that are outgoing from the internal sides of the layer boundaries (Fig. 1). They each consist of internally reflected energy and externally incident radiation transmitted through a boundary.

Boundary conditions

Boundary conditions are required for radiation and for heat conduction coupled with external convection. Radiation passes out of the layer from within a material. There is no emission at the boundaries, which are planes without volume; hence, there are no radiation terms in the surface convective boundary conditions. The conduction–convection boundary conditions at $x = 0$ and $x = D$ for all times were:

$$-\kappa\frac{\partial T}{\partial x}|x = 0 = h_1[Tg_1 - T(x = 0,\theta)] \tag{3a}$$

$$-\kappa\frac{\partial T}{\partial x}|x = D = h_2[T(x = D,\theta) - Tg_2] \tag{3b}$$

The radiation boundary conditions were developed in a manner described previously[25,26]; they were required for the time-dependent fluxes $\tilde{q}_{0,b}(\tau)$ and $\tilde{q}_{0,c}(\tau)$ in eq. (2). Using the reflectivity on both sides of the boundary surfaces, each $\tilde{q}_0$ was composed of transmitted and reflected portions: $\tilde{q}_{0,b} = (1 - \rho_a)\tilde{q}_{r1} + \rho_b\tilde{q}_{i,b}$ and $\tilde{q}_{0,c} = (1 - \rho_a)\tilde{q}_{r2} + \rho_c\tilde{q}_{i,c}$ (Fig. 1). The boundaries were assumed to be sufficiently rough that all reflections were diffuse. The incident fluxes within the layer, $\tilde{q}_{i,b}$ and $\tilde{q}_{i,c}$, consisted of energy leaving the opposite boundary and being attenuated through the layer and energy incident at the boundary as a result of emission within the layer. Obtained from the radi-

ative flux equation, which is the integral of eq. (2), they are, as detailed in Weston and Hauth,[12]

$$\tilde{q}_{0,b}(\tau) = \frac{C_1(\tau) + A_b C_2(\tau)}{1 - A_b A_c} \tag{4a}$$

$$\tilde{q}_{0,r}(\tau) = \frac{C_2(\tau) + A_c C_1(\tau)}{1 - A_b A_c} \tag{4b}$$

where, for conditions including incident external radiation,

$$A_b = 2\rho_b E_3(\kappa_D) \tag{4c}$$

$$A_c = 2\rho_c E_3(\kappa_D) \tag{4d}$$

$$C_1(\tau) = (1 - \rho_d)\tilde{q}_{r1} + 2n^2\rho_b\kappa_D \int_1^4 t^4(X,\tau) E_2(\kappa_D X) dX \tag{4e}$$

$$C_2(\tau) = (1 - \rho_d)\tilde{q}_{r2} + 2n^2\rho_c\kappa_D \int_1^4 t^4(X,\tau) E_2[\kappa_D(1 - X)] dX \tag{4f}$$

The specific case of black surroundings would use $\tilde{q}_{r1} = t_{s_1}^4$ and $\tilde{q}_{r2} = t_{s_2}^4$.

Numerical solution procedure

The numerical solution developed in this work combines approaches and ideas from the numerical procedure detailed previously,[3] to which modifications were made for external radiation and convection. Trapezoidal integration of $dt/d\tau$ over a small Δt was used to incrementally increase the temperature over time to give $\Delta t \equiv t_{n+1} - t_n \approx (\Delta\tau/2)\,[(dt/d\tau)_{n+1} + (dt/d\tau)_n]$.

The second derivative of temperature at $\tau + \Delta\tau$ (at index $n + 1$) can be written in terms of $t(\tau)$, at index n, and Δt as $(dt^2/dx^2)_{n+1} = \partial\Delta t/\partial X^2 + \partial^2 t_n/\partial X^2$. The radiative source at $\tau + \Delta\tau$, $R(\tau + \Delta\tau) \equiv R_{n+1}$, can be expressed in terms of $R(\tau) \equiv R_n$ by $R_{n+1} \equiv R_n(\partial R/\partial t)_n \Delta t$. By using eq. (1) to eliminate $\partial t/\partial\tau$ in the Δt relation and applying the two preceding relations, an equation for Δt was obtained:

$$\left[1 + \frac{\Delta\tau}{2}\left(\frac{\partial R}{\partial t}\right)_n - \frac{N\Delta\tau}{2}\frac{\partial^2}{\partial X^2}\bigg|_n\right]_{\Delta t} = \Delta\tau\left[N\left(\frac{\partial^2 t}{\partial X^2}\right)_n - R_n\right] \tag{5}$$

The subscript i specifies the X location ($i = 1$ at $X = 0$, $i = M$ at $X = 1$). Relations were now developed to obtain $\Delta t(X_i) = \Delta t_i$ at X_i at τ_n; the temperatures at τ_{n+1} were then $\tau_{n+1}(X_i) = \tau_n(X_i) + \Delta t(X_i)$.

Because all terms on the right-hand sides of the preceding equations in this section are at τ, corresponding to the index n, this subscript is omitted in the following.

To obtain a solution, relations were needed in eq. (5) for $\partial/\partial X^2$ at the internal grid points of the layer and at the boundaries. For non-uniform-sized increments ΔX_i^- and ΔX_i^+ in the negative and positive directions about each X_i, the standard second-derivative discretization was substituted into eq. (5) to obtain an equation for Δt_i at the interior points $2 \le I \le M - 1$.

$$-\frac{N\Delta\tau}{\Delta X_i^-(\Delta X_i^+ + \Delta X_i^-)}\Delta t_{i-1} + \left[1 + \frac{\Delta\tau}{2}\left(\frac{\partial R}{\partial t}\right)_i + \frac{N\Delta\tau}{\Delta X_i^- \Delta X_i^-}\right]\Delta t_i - \frac{N\Delta\tau}{\Delta X_i^+(\Delta X_i^+ + \Delta X_i^-)}\Delta t_{i+1} = \Delta\tau\left\{-\frac{2N}{\Delta X_i^+ + \Delta X_i^-} - \left[\frac{t_{i+1}}{\Delta X_i^+} - \left(\frac{\Delta X_i^+ + \Delta X_i^+}{\Delta X_i^+ \cdot \Delta X_i^-}\right)t_i + \frac{t_{i-1}}{\Delta X_i^-}\right] - R_i\right\} \tag{6}$$

To account for convection at each boundary, eq. (6) was replaced by special forms developed from the boundary conditions in eqs. (3a) and (3b). At $I = 1$, by using the definition of Δt, eq. (3a) in dimensionless form, $-(\partial t/\partial X)|_{i=1} = (H_1/4N)(tg_1 - t_1)$, could be written in terms of Δt by taking the difference in values at $\tau + \Delta\tau$ and τ:

$$-\frac{\partial\Delta t}{\partial X}\,|i = 1 = (H_1/4N)\Delta t_1 \tag{7}$$

In the finite difference procedure $\partial^2\Delta t/\partial^2 X^2$ is needed at $i = 1$ for use in eq. (5).

Expanding for either $\xi = \Delta t$, or t of about $i = 3/2$, resulted in

$$\frac{\partial\xi}{\partial X}\,|_{i=3/2} = \frac{\partial\xi}{\partial X}\,|_{i=1} + \frac{\partial\xi^2}{\partial X^2}\,|_{i=1}\frac{\Delta X_1^+}{2} + \cdots \tag{8}$$

The quantity $(\xi_2 - \xi_1)/\Delta X_1^+$ was substituted in eq. (8) for the first derivative at $I = 3/2$, and either eq. (7) or (3a) was substituted for $\partial\Delta t/\partial X$ and $\partial t/\partial X$ at $i = 1$, which, after rearrangement, produced the following:

$$\frac{\partial^2\Delta t}{\partial X}\,|_{i=1} = \frac{2}{\Delta X_1^+}\left[\frac{\Delta t_2 - \Delta t_1}{\Delta X_1^+} - \frac{H_1}{4N}\Delta t_1\right. \tag{9a}$$

$$\frac{\partial^2 t}{\partial X^2}\Big|_{i=1} = \frac{2}{\Delta X_1^+}\left[\frac{t_2 - t_1}{\Delta X_1^+} - \frac{H_1}{4N}(t_{g1} - t_1)\right] \quad (9b)$$

For $I = 1$, eqs. (9a) and (9b) were substituted into eq. (5) to give, after rearrangement,

$$\left[1 + \frac{\Delta\tau}{2}\left(\frac{\partial R}{\partial t}\right)_1 + \frac{N\Delta\tau}{(\Delta X_1^+)^2}\left(1 + \frac{H_1\Delta X_i^+}{4N}\right)\right]\Delta t_1 - \frac{N\Delta\tau}{(\Delta X_1^+)^2}\Delta t_2 = \Delta\tau\left[\frac{2N}{(\Delta X_1^+)^2}(t_2 - t_1) + \frac{H_1}{2\Delta X_1^+}(t_{g1} - t_1) - R_1\right], \; i = 1 \quad (10a)$$

Similarly, at $i = M$, these substitutions gave:

$$-\frac{N\Delta\tau}{(\Delta X_M^-)^2}\Delta t_{M-1} + \left[1 + \frac{\Delta r}{2}\left(\frac{\partial R}{\partial t}\right)_M + \frac{N\Delta\tau}{(\Delta X_M^-)^2}\left(1 + \frac{H_2\Delta X_M^-}{4N}\right)\right]\Delta t_M = \Delta r\left[\frac{2N}{(\Delta X_M^-)^2}(t_{M-1} - t_M) + \frac{H_2}{2\Delta X_M^-}(t_{g2} - t_M) - R_M\right] \quad (10b)$$

Eqs. (6) and (10) provide a tridiagonal system for obtaining $\Delta t_1, \Delta t_2, \Delta t_3, \ldots \Delta t_M$; the coefficients are given in the appendix.

For the b_i coefficients, $\partial R/\partial t$ was needed. From eq. (2), the following equation was given:

$$\frac{\partial R}{\partial t}\Big|_x = 4n^2\kappa_D t^3(X,\tau) - \left[\frac{\kappa_D}{2}\left\{\frac{d\tilde{q}_{0,b}(\tau)}{d\tau}E_2(\kappa_D X) + \frac{d\tilde{q}_{0,c}(\tau)}{d\tau}E_2[\kappa_D(1 - X)]\right\} + 2n^2\kappa_D^2\int_o^1 t^3(X^+,\tau)\frac{\partial t(X^+,\tau)}{\partial\tau}\Big|_{x^+}E_1(\kappa_D|X^+ - X|)dX^+\right]\cdot\left[\frac{\partial t(X,\tau)}{\partial\tau}\Big|_x\right]^{-1} \quad (11)$$

From eq. (4), the time derivatives of $\tilde{q}_{0,b}$ and $\tilde{q}_{0,c}$ in eq. (11) were:

$$\frac{d\tilde{q}_{0,b}(\tau)}{d\tau} = \frac{(dC_1(\tau)/d\tau) + A_b(dC_2(\tau)/d\tau)}{1 - A_bA_c}$$

$$\frac{d\tilde{q}_{0,c}(\tau)}{d\tau} = \frac{(dC_2(\tau)/d\tau) + A_c(dC_1(\tau)/d\tau)}{1 - A_bA_c} \quad (12)$$

where

$$\frac{dC_1(\tau)}{d\tau} = 8n^2\rho_b\kappa_D\int_0^1 t^3(X,\tau)\frac{\partial t(X,\tau)}{\partial\tau}\Big|_x E_2[\kappa_D X)dX\frac{dC_2(\tau)}{d\tau}$$

$$= 8n^2\rho_c\kappa_D\int_{II}^I t^3(X,\tau)\frac{\partial t(X,\tau)}{\partial\tau}\Big|_x E_2[\kappa_D(1 - X)]dX \quad (13)$$

The tridiagonal array was solved using an algorithm described previously.[27,28] At each X_i, Δt was added to t_i to advance the temperature to the next time.

To evaluate the radiative source term $[R(t)]$, eq. (2), and its derivative $(\partial R/\partial t)$, eq. (11), an accurate integration method was required. A special treatment as described previously[29] was used as X^* approached X because $E_1(0) = \infty$. An analytical integration was used for a very small region about the singularity, and Gaussian integration (using an IMSL subroutine) was used starting at this very small distance from the singularity. Values of the functions at the unevenly spaced locations in the Gaussian subroutine were found from the grid point values by cubic spline interpolation. By trying various values and numbers of grid points, it was found that increments across the layer gave accurate results for the κ_D considered here. Small values of $\Delta X = 0.1$ were used for 10 increments near the boundaries, where temperature variations can be large. To avoid numerical instabilities that can arise for a complex integrodifferential equation as given by eqs. (1) and (2), a small time step, $\Delta\tau = 0.005$, was used for the first 20 $\Delta\tau$; after that $\Delta\tau = 0.01$ was used. In most instances the temperature distributions for $\tau = 1.5$ were less than 1% from steady state.

Transient energy balance

The transient temperature distributions were used in an overall energy balance to check numerical solution accuracy at each time step.

The instantaneous energy rate incident by radiation and added by convection is in dimensionless form, $\tilde{q}_{r1} + \tilde{q}_{r2} + H_1[t_{g1} - t(0,\tau)] + H_2[t_{g2} - t(1,\tau)]$. This must equal the sum of radiative energy reflected and emitted by the layer and the transient rate of energy storage. The reflected energy is $\rho_a\tilde{q}_{r1} + \rho_d\tilde{q}_{r2}$. The instantaneous radiative flux leaving through both boundaries is $(1 - \rho_b)\tilde{q}_{i,b} + (1 - \rho_c)\tilde{q}_{i,c} = [(1 - \rho_b)/\rho_b][\tilde{q}_{0,b} - (1 - \rho_a)\tilde{q}_{r1}] + [(1 - \rho_c)/\rho_c][\tilde{q}_{0,c} - (1 - \rho_d)\tilde{q}_{r2}]$. This was evaluated using $\tilde{q}_{0,b}$ and $\tilde{q}_{0,c}$ from eq. (4). The transient energy storage rate was obtained from $(4/\Delta\tau)[t_m(\tau + \Delta\tau) - t_m(\tau)]$, where $t_m(\tau)$ is the instantaneous integrated mean temperature across the layer. The overall energy balance was satisfied within 0.5% through the transient calculations.

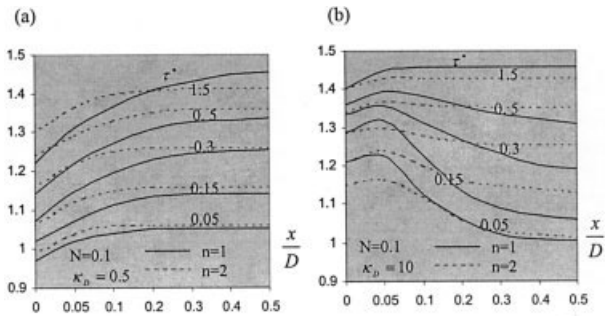

Figure 2 Effect of refractive index on transient temperature distribution in a layer initially at a uniform temperature after exposure to external radiation and convective cooling: (a) optical thickness (κ) = 0.5; (b) κ, = 10.

RESULTS AND DISCUSSION

The transient temperature distributions given here started from a uniform initial temperature, $T(X,0) = T_i$, so $t(X,0) = 1$. The results shown in Figure 2 indicate that the external radiation and convection conditions were symmetric on both sides of the layer, so the transient temperatures were symmetric. The distributions are for one-half of the layer. The results are the measurements at five points across the transient distribution; the distribution for the longest time was at or very close to a steady state.

The results shown in Figure 2 demonstrate the effect on cooling an advanced polymer layer of coating its boundaries to make them opaque and unable to admit radiant transmission. This shows how coatings can be used to regulate heat-transfer processes during manufacturing with plastics. Equal convective cooling was provided at both surfaces. The results for the temperatures predicted to include both internal radiation and conduction (solid lines) were compared with those for internal heat conduction only (dashed lines).

The conduction–radiation parameter was an attempt to characterize the radiative importance of conduction and radiation. Figure 2(a) shows that the N was small enough (0.05) for internal radiation to significantly affect the temperatures, making them more uniform during transient cooling. The layer also cooled more rapidly with combined radiation and conduction. Figure 2(b) shows that the conduction–radiation parameter decreased to $N = 0.005$; therefore, conduction had less effect, and the layer cooled somewhat more slowly. Internal radiation made the temperatures much more uniform than with conduction alone. Moreover, radiative heating at a distance erased frontier gradients from conduction, and as a result very uniform long-lasting temperature profiles were established after shorter intervals.

Figure 3 shows the changed conditions at the boundaries. The layer was heated on the hot side by a radiative flux equal to that from black surroundings at $T_{s1} = 1.5\ T_i$.

There was no convective cooling on the hot side ($H_1 = 0$). Cooling occurred on the cold side ($X = 1$) by convection ($H_2 = 1$ and $T_{g2} = 0.5\ T_i$) and by radiation to the black surroundings ($T_{s2} = 0.5\ T_i$). The results shown in Figure 2(a,b) are for optical thicknesses of 2 and 10, respectively. For the results shown in Figure 3(a), the κ_D was 2 and optical thickness was such that the maximum internal radiative effect was expected. On the hot-side boundary the lack of convective cooling resulted in a zero temperature gradient because radiation left from inside the layer, not from its surface.

Figure 3(b) shows the κ_D increased to 10, with more absorption of incident radiation near the boundary. Early in the transient temperature distribution there was a strong temperature rise near the hot boundary, whereas temperatures decreased substantially at the boundary that was convectively cooled. Each part of Figure 3(b) shows results for $n = 1$ and 2. Increasing n was not as effective in equalizing temperature as in Figure 3(a) because radiative transfer across the layer, as augmented by internal reflections, was reduced by the increased κ_D.

For the results shown in Figure 4, it was assumed that initially the STM layer was fitted with opaque frontiers and stood at uniform temperature, T_i. One of its boundaries was suddenly held at the fixed temperature, T_{s1}, up to the steady state. The following results were computed for the temperature conditions $T_{s1} =$ 750 K and $T_{s2} = 1500$ K. So the problem had to be solved in these conditions:

$$t_{s1}(X,t = 0) = 1 \quad 0 \le X \le 1 \tag{14}$$

Temperature and flux profiles of the layer bounded by the black frontiers are shown in Figure 2(a–c) for dimensionless time, τ, and for the conductive–radiative coupling parameters $N = 0.5$, 0.05, and 0.005, corresponding to a thickness of 1 cm. For small dimensionless time values, thermal gradients were elevated

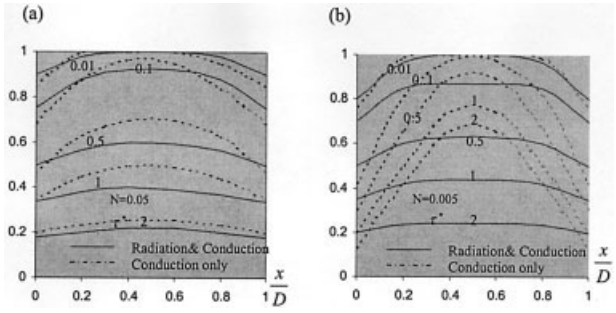

Figure 3 Transient temperature distribution for cooling a polymer layer showing comparison of combined radiation–conduction with conduction only ($Ts_1 = Ts_2$ 1500 K; $h_1D/k = h_2D/k = 0.1$): (a) conduction–radiation parameter, $N =$ 0.05; (b) conduction–radiation parameter, $N = 0.005$.

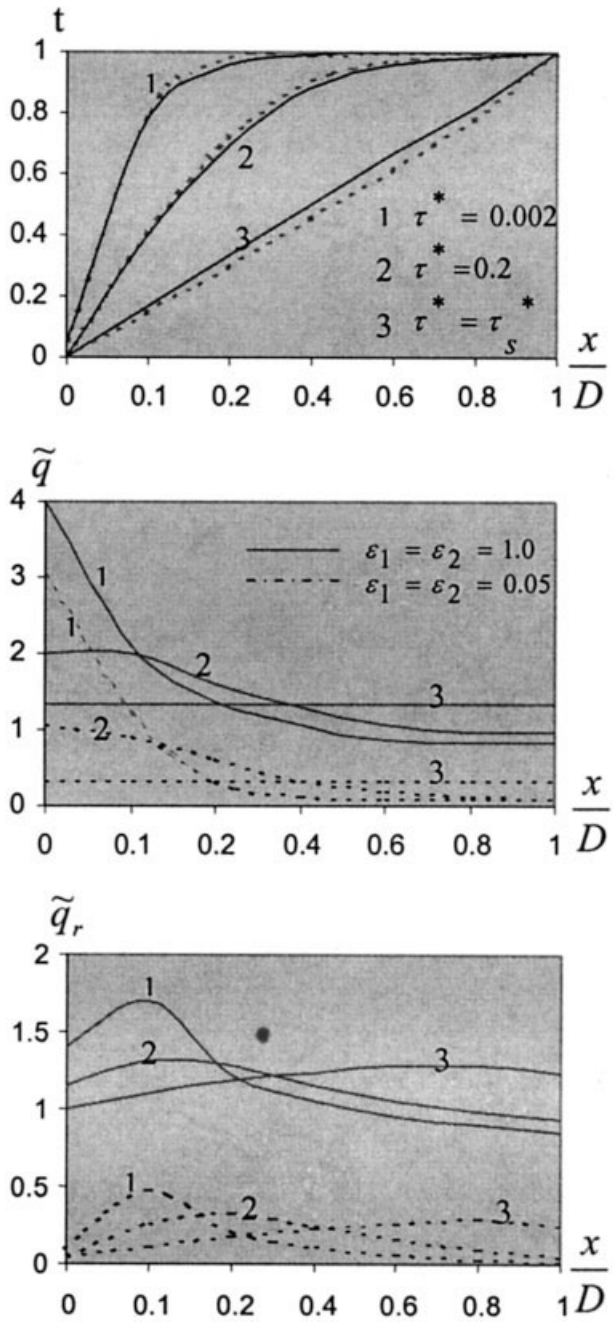

Figure 4 Effect of change in radiative properties for a plastic layer of $d = 1$ cm for fixed boundary temperatures.

in the vicinity of the cooled boundary, and the conduction phenomenon was dominant. Profiles of radiative flux displayed a maximum that appeared near the cooled part of the slab and a radiative cooling of its major inner part.

At intermediate-length dimensionless times, that is, long before the steady state, the coupling produced drastic cooling of the zone—never influenced by the hot boundary—all the more so as N was weak; for example, if N was 0.005, a heat sink speared near the hot interface, which lost more energy by radiation that it gained. The position of the radiative flux maximum moved toward the hot surface, indicating expansion of the radiantly heated zone.

In the layer, absorption of radiation at a distance increased when N decreased, and consequently the mean temperature increased; thus, a shorter time was needed to reach the steady state. In the steady state, thermal gradients increased near the boundaries, involving higher conductive exchanges and leading to the well-known S-shaped temperature profile of simultaneous radiative–conductive heat transfer. When N was very small, heat transfer was carried out almost purely by radiation, and temperature profiles were close to the slipping effect.

The results of examining modifications in the shapes of the absorption spectra shape (Spectra A and 130, reported below) were for a 10-cm-thick slab ($N = 0.005$) bounded by black coating and are represented in Figure 3.

With shorter times, there was some difference in the temperature profiles of the two materials in the hot part of the layer. Isochrones for spectrum A decreased at a faster rate than those for spectrum B. Flux density profiles were more sensitive. It can be observed in Figure 3 that with short durations differences between spectra A and B in the importance of radiative transfer favored the most transparent material. For thicker layers, this trend was enhanced.

The effects on the flux profiles of a change in the radiative characteristics of the frontiers—passing from a system with two black frontiers to a system with almost fully reflecting ones—are shown in Figure 4 for a 1-cm-thick nongray material of spectrum A. Although the temperature distributions were not strongly modified for that thickness ($N = 0.05$), the radiative flux profiles showed a very important decrease in the magnitude of radiative flux—by a factor of 3 at the maximum for shorter times—because of less effective cooling and heating at a distance. At the two slab extremities radiative flux tended toward zero because the net radiative flux (leaving flux − incident flux) moved toward a null value as the emissivity of the frontiers vanished. So when multiple reflections were taken into account, total heat flux was correspondingly weaker than with the two black frontiers.

For the results shown in Figures 5–7, the conditions at the boundaries were changed. The solution was now used to solve more complex radiative–conductive heat transfer problems—those of a plane layer of an STM the temperature of which was prescribed on one interface with the opposite face subjected to radiative–convective heat exchanges. Two examples are given of treatment by varying the fixed temperature.

In the first example, the prescribed temperature was the initial one, $T_{s2} = T_i = 1500$ K; on the other face the slab could exchange heat with the environment, the temperature of which was $T_{s1} = 750$ K, by both radi-

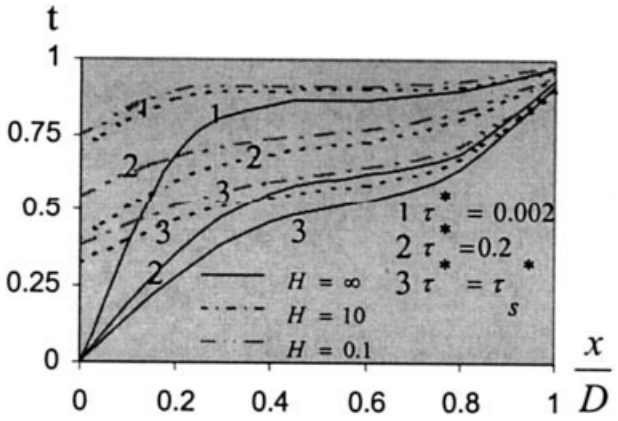

Figure 5 Temperature profiles at various times in mixed conditions for various radiation–conduction parameters.

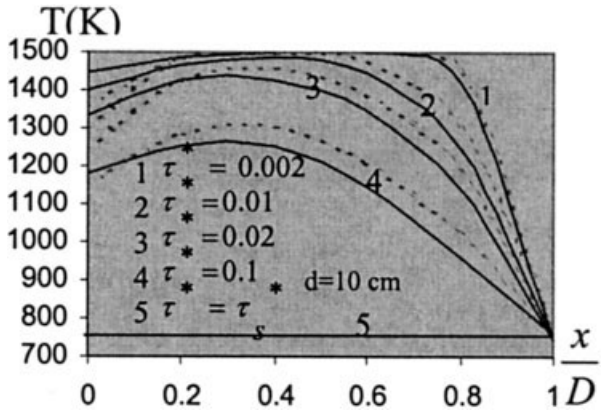

Figure 7 Temperature profiles for mixed conditions for a sudden drop in temperature [Ts_1, $d = 1$ (spectrum A)] for opaque/semitransparent frontiers compared with pure conductive exchanges.

ative cooling and natural convection controlled by several convection–radiation parameters. The layer was 10-cm- thick slab (corresponding to $N = 0.005$) of spectrum A. The hot face was opaque and coated with a reflecting layer ($\rho = 0.9$); for the other face, two radiative boundary conditions were selected, either semitransparent or opaque (emissivity, $\varepsilon = 0.94-0.96$).

The solution of this problem was achieved by considering the initial and boundary condition as follow:

$$\text{Boundary condition: } t_{s1} = 0.5 \text{ and } t_{s2} = 1 \quad (15a)$$

$$\text{Initial condition: } t(X, t = 0) = 1 \quad (15b)$$

The transient and permanent temperature profiles are plotted in Figure 5 for the two opaque frontiers. When convective exchange was poor, the temperature setting for the cold face was much higher than the environmental one. With more effective convective dissipation, the different isochrones moved toward lower temperatures. With direct, perfect contact between the cooled face and the ambient medium, the resulting temperature profile was of the same type as that shown in Figure 2(c).

In the steady state, a low temperature gradient at the free interface in the presence of small convective effects was observed.

If radiative heat flux profiles were very different with short increments of time, they were very close and uniform in the steady state, except in the hot zone near the reflecting frontier.

In the second example, the prescribed temperature was half that of the initial one, $T_{s2} = 750$ K. The thermal boundary conditions were therefore similar to those described above except that t_{s2} was 0.50 K. The chosen radiative conditions were those of a slab limited by an isothermal opaque frontier, determined by a metallic bath of low emissivity, with a semitransparent interface with vitreous reflections on the opposite side. The evolution of the temperature distribution within the plastic layer is displayed in Figure 7 for five cooling times during the cooling process. At early times, the region of the layer in direct contact with the metallic bath lost only its energy conduction, although the free interface was cooled by convection. The central part of the layer, still at high temperature, exchanged heat by radiation with the cold parts. As a result, the mean temperature was decreasing, as was the magnitude of the gradient. At very long times, the temperature of the layer became uniform except near the zone, which was still influenced by the cold frontier. Also, Figure 7(a) shows a comparison of this case with the pure conductive case.

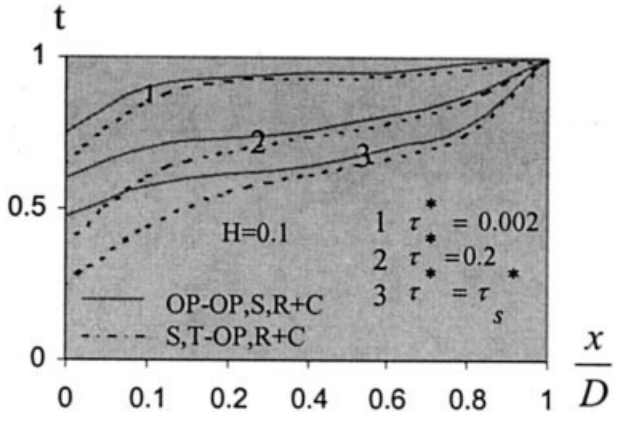

Figure 6 Temperature profiles for mixed conditions ($Ts_1 = T_{initial}$): comparison of opaque/opaque and semitransparent/opaque frontiers.

CONCLUSIONS

On the basis of my previous works, the implicit finite deference solution was extended to the study of transiently coupled radiation and conduction in a layer of

TABLE I
Optical Characteristics of the Different Plastics Used

$\lambda(\mu m)$	n	Spectrum A $a_\lambda(m^{-1})$	Spectrum B $a_\lambda(m^{-1})$	$\lambda(\mu m)$	n	$\rho_1=\rho_2$	Spectrum C $a_\lambda(m^{-1})$
0.55–3	1.55	10	2.5	0.55–1.0	1.5	0.045	10
0.55–3	1.55	10	2.5	1.0–3.0	1.5	0.045	100
3.0–5.0	1.55	1000	250	3.0–5.3	1.5	0.045	1000
4.5–50	1.55	5000	1250	4.5–10.5	1.5	0.08	10000
4.5–50	1.55	5000	1250	10.5–50	1.8	0.15	10000

advanced polymer fiber. The solution presented here, whose development fully took into account all the parameters involved in the problem, can be used to obtain predictions of temperature and heat flux profiles within a polymer layer for realistic absorption infrared spectra and various thermal nonequilibrium situations of physical and technological interest.

The developed numerical method is stable for any ratio of radiative to conductive heat transfer and any emissivity of the boundaries. The high precision of its temperature profile and heat flux allows extreme constellations to be considered for parameter studies.

NOMENCLATURE

- a_k absorption coefficient of the layer, relative to spectral band k (m^{-1})
- C specific heat of radiating medium (Ws kg^{-1} K^{-1})
- D thickness of radiating layer (m)
- $E_1,\ldots E_n$ exponential integral functions
- h convective heat transfer coefficient (Wm^{-2} K^{-1})
- H convection-radiation parameter, $h/(\sigma T_i^3)$
- κ thermal conductivity of the layer (Wm^{-1} K^{-1})
- n refractive index of the layer
- N conduction–radiation parameter, $\kappa/(4\sigma T_i^3 D)$
- q heat flux (Wm^{-2})
- $\tilde{q}$ dimensionless flux, $q/(\sigma T_i^4)$
- q_r radiative heat flow per unit area and time (Wm^{-2})
- qr_1, qr_2 external radiative fluxes incident on sides of layer (Wm^{-2})
- R radiative source term in energy equation
- t dimensionless temperature, T/T_I
- T absolute temperature (K)
- T_i initial temperature of semitransparent layer (K)
- T_m integrated mean temperature (K), $t_m = T_m/T_i$
- T_s temperature of surroundings (K), $t_s = T_s/T_i$
- x coordinate in direction across layer (m)
- X dimensionless coordinate, x/D.

Greek symbols

- δ half thickness of the layer
- $\varepsilon_1,\varepsilon_2$ emissivity of the layer at $x = 0$ and $x = D$, respectively
- ε_{ut} emissivity of layer at uniform temperature
- θ time (s)
- κ_D optical thickness of layer (aD)
- ρ density of layer [kg/m^3], surface reflectivity
- σ Stefan–Boltzmann constant (Wm^{-2} K^{-4})
- τ dimensionless time, $(4\sigma T_i^3/\rho CD)\theta$
- τ_s steady-state dimensionless time

Subscripts

- $a\ b\ c\ d$ interfaces of layer (Fig. 1)
- g gas for convection at boundary
- i initial condition: incoming radiation
- i ith X location
- M total number of X grid points
- n at nth time increment
- o outgoing radiation
- s surrounding environment
- ss at steady state
- ut uniform temperature condition
- 1,2 external conditions on two sides of layer

Superscripts

- c, r, t conduction, radiation and total respectively
- s specular reflection

References

1. Sadooghi, P.; Aghanajafi, C. Radiat Eff Defects Solids 2004, 159, 61
2. Sadooghi, P.; Aghanajafi, C. J Fusion Energy 2004, 22, 59.
3. Sadooghi, P. J Vinyl Additive Technol 2005, 11, 28.
4. Sadooghi, P. J Quant Spectrosc Radiat Transf 2005, 93, 461.
5. Sadooghi, P. J Quant Spectrosc Radiat Transf 2005, 92, 403.
6. Sadooghi, P.; Aghanajafi, C. Infra Phys Technol 2006, 47, 278.
7. Sadooghi, P.; Aghanajafi, C. J Reinforced Plast Comp 2005, 24, 1655.
8. Siegel, R.; Howell, J. R. Thermal Radiation Heat Transfer. 3rd ed.; Hemisphere: Washington, DC, 1992; Chapter 16.

9. Viskanta, R. In Proceedings of the Seventh International Heat Transfer Conference, Hemisphere: Washington, DC, 1982; Vol. 1, p 103.
10. Bathla, P. S.; Viskanta, R. Appl Sci Res 1968, 19, 182.
11. Viskanta, R.; Bathla, P. S. Z Angew Math Phys (ZAMP) 1967, 18, 353.
12. Weston, K. C.; Hauth, J. L. J Heat Transf 1973, 95, 357.
13. Ping, T. H.; Lallemand, M. Int J Heat Mass Transf 1989, 32, 795.
14. Lii, C. C.; Ozisik, M. N. Int J Heat Mass Transf 1972, 15, 1175.
15. Tsai, C. F.; Nixon, G. Numer Heat Transf 1986, 10, 95.
16. Siegel, R. J Heat Transf 1987, 109, 159.
17. Song, B.; Viskanta, R. J Thermophys Heat Transf 1990, 4, 311.
18. Siegel, R. J Thermophys Heat Transf 1992, 77.
19. Reiss, H. Radiative Transfer in Nontransparent Dispersed Media; Springer: Berlin, 1988.
20. Viskanta, R.; Menguc, M. P. Appl Mech Rev 1988, 42, 241.
21. Reiss, H. High Temp High Press 1990, 22, 481.
22. Kaganer, M. G. Heat and Mass Transfer in Low Temperature Equipment; Energiya: Moscow, 1979; Chapter 2.
23. Siegel, R. J Thermophys Heat Transf 1992, 6, 77.
24. Siegel, R. J Thermophys Heat Transf 1995, 9, 55.